Optical microscopy of 3D carpet cloaks:ray-tracing calculations

Tolga Ergin,[1,*] Jad C. Halimeh,[2,3] Nicolas Stenger,[1] and Martin Wegener[1,4]

[1] *Institut für Angewandte Physik and DFG-Center for Functional Nanostructures (CFN), Karlsruhe Institute of Technology (KIT), D-76128 Karlsruhe, Germany*
[2] *Max-Planck-Institut für Quantenoptik, D-85748 Garching, Germany*
[3] *Fakultät für Physik, Ludwig-Maximilians-Universität, D-80799 München, Germany*
[4] *Institut für Nanotechnologie, Karlsruhe Institute of Technology (KIT),Postfach 3640, D-76021 Karlsruhe, Germany*
tolga.ergin@kit.edu

Abstract: In a recent publication (T. Ergin *et al.*, Science **328**, 337 (2010)), three-dimensional broadband dielectric carpet cloaks have been fabricated and experimentally characterized by optical bright-field and dark-field microscopy using unpolarized light from an incandescent lamp. A direct comparison with theory has not been provided so far. In the present work, we treat the carpet cloak as well as the entire optical microscope within the ray-optics approximation and the cloak within the effective-medium approximation. We find good qualitative agreement between experimental results and our calculations.

OCIS codes: (080.0080) Geometric optics; (230.3205) Invisibility cloaks; (160.3918) Metamaterials; (080.2710) Inhomogeneous optical media.

References and links

1. J. B. Pendry, D. Schurig, and D. R. Smith, "Controlling electromagnetic fields," Science **312**(5781), 1780–1782 (2006).
2. U. Leonhardt, "Optical conformal mapping," Science **312**(5781), 1777–1780 (2006).
3. J. Li, and J. B. Pendry, "Hiding under the carpet: a new strategy for cloaking," Phys. Rev. Lett. **101**(20), 203901 (2008).
4. V. M. Shalaev, "Physics. Transforming light," Science **322**(5900), 384–386 (2008).
5. H. Chen, C. T. Chan, and P. Sheng, "Transformation optics and metamaterials," Nat. Mater. **9**(5), 387–396 (2010).
6. D. Schurig, J. J. Mock, B. J. Justice, S. A. Cummer, J. B. Pendry, A. F. Starr, and D. R. Smith, "Metamaterial electromagnetic cloak at microwave frequencies," Science **314**(5801), 977–980 (2006).
7. R. Liu, C. Ji, J. J. Mock, J. Y. Chin, T. J. Cui, and D. R. Smith, "Broadband ground-plane cloak," Science **323**(5912), 366–369 (2009).
8. J. Valentine, J. Li, T. Zentgraf, G. Bartal, and X. Zhang, "An optical cloak made of dielectrics," Nat. Mater. **8**(7), 568–571 (2009).
9. L. H. Gabrielli, J. Cardenas, C. B. Poitras, and M. Lipson, "Silicon nanostructure cloak operating at optical frequencies," Nat. Photonics **3**, 461–463 (2009).
10. J. H. Lee, J. Blair, V. A. Tamma, Q. Wu, S. J. Rhee, C. J. Summers, and W. Park, "Direct visualization of optical frequency invisibility cloak based on silicon nanorod array," Opt. Express **17**(15), 12922–12928 (2009).
11. I. I. Smolyaninov, V. N. Smolyaninova, A. V. Kildishev, and V. M. Shalaev, "Anisotropic metamaterials emulated by tapered waveguides: application to optical cloaking," Phys. Rev. Lett. **102**(21), 213901 (2009).
12. J. C. Halimeh, T. Ergin, J. Mueller, N. Stenger, and M. Wegener, "Photorealistic images of carpet cloaks," Opt. Express **17**(22), 19328–19336 (2009).
13. T. Ergin, N. Stenger, P. Brenner, J. B. Pendry, and M. Wegener, "Three-dimensional invisibility cloak at optical wavelengths," Science **328**(5976), 337–339 (2010).
14. H. F. Ma, and T. J. Cui, "Three-dimensional broadband ground-plane cloak made of metamaterials," Nature Commun. **1**(3), 1–6 (2010).
15. B. Zhang, T. Chan, and B.-I. Wu, "Lateral Shift Makes a Ground-Plane Cloak Detectable," Phys. Rev. Lett. **104**(23), 233903 (2010).

1. Introduction

Invisibility cloaking appeals to scientists and laymen alike by the mere fact that it was commonly believed impossible until a few years ago. Scientifically, it can be viewed as a demanding benchmark example for the much broader and far-reaching concepts of

#133154 - $15.00 USD Received 10 Aug 2010; revised 1 Sep 2010; accepted 2 Sep 2010; published 10 Sep 2010

transformation optics [1–3]. A more complete list of references can be found in the recent reviews [4,5]. Meanwhile, early experiments on invisibility cloaking in two-dimensional waveguide geometries at microwave [6,7] and at optical frequencies [8–11] have been presented. In these experiments, however, the notion "invisibility cloaking" has to be taken with a grain of salt as the so-called "invisible" becomes immediately visible when inspected from the (normal) third dimension. Recently, we have discussed a three-dimensional version [12,13] of the carpet cloak that has originally been introduced for a two-dimensional setting [3]. Our experiments [13] using bright-field and dark-field optical microscopy and spectroscopy with unpolarized light and with large-numerical-aperture microscope lenses (corresponding to large angular spread of the light in three dimensions) have further validated the ideas underlying transformation optics even in three dimensions. Yet more recently, another research group has also presented a related three-dimensional carpet cloak, albeit operating at microwave frequencies [14].

In this contribution, we aim at presenting calculations that mimic the microscope imaging process in quite some detail and that allow for a direct comparison with our previously published experimental data. As complete wave-optics calculations including the actual measurement setup (i.e., the entire optical microscope) and the precise cloaking nanostructure are presently out of reach for us, we restrict ourselves to ray tracing of bright-field and dark-field images of structures without and with cloak within the effective-medium description.

2. Experiment

Let us start by very briefly recalling our previously published experiments [13] on the three-dimensional version of the carpet cloak. In these experiments [13], we have considered a bump in a metallic film, the outline of which follows $y(x) = h \cos^2(\pi x/w)$ for $|x| \leq w/2$ and zero otherwise. The height of the bump is $h = 1.25$ µm and its full width is $w = 13$ µm. The bump is translationally invariant along the z-direction. The total extent of the structure is 90 µm in the x-direction, 10 µm in the y-direction, and 30 µm in the z-direction [13]. It is located on a glass substrate with a thickness of 170 µm. To hide the bump, the refractive index profile is calculated using the quasi-conformal mapping outlined in Ref. 3. A reference refractive index [3] of $n = 1.2$ is used [13]. The result of our own calculation along these lines and for the above parameters is shown in Fig. 1.

In our experiments [13], this index profile is approximated by locally varying the volume filling fraction of a three-dimensional polymer woodpile photonic crystal that is used in the long-wavelength limit. Obviously, 100% filling fraction delivers the index of the polymer, i.e., $n = 1.52$, and 0% filling fraction the index of air, i.e., $n = 1$. This blueprint is fabricated using three-dimensional direct laser writing [13]. After development, the top is coated with gold in a sputter chamber. Further details on these samples can be found in Ref. 13.

For the optical characterization, we simply look at the samples with a microscope in either bright-field or dark-field mode [13]. The employed dedicated home-made microscope setup is schematically shown in Fig. 2. The sample is illuminated by unpolarized incoherent white light from a light bulb and imaged by a single reflective Cassegrain microscope objective lens with focal length $f = 5.41$ mm and numerical aperture $NA = 0.5$ onto the image plane. The magnification factor is $m = -80$. "Bright-field mode" refers to the case that the optical axis and the sample surface normal are parallel, "dark-field mode" to the case that the two include an angle, in which case a planar metal surface would appear dark in the image (see Fig. 1). Further details can be found in Ref. 13.

#133154 - $15.00 USD Received 10 Aug 2010; revised 1 Sep 2010; accepted 2 Sep 2010; published 10 Sep 2010

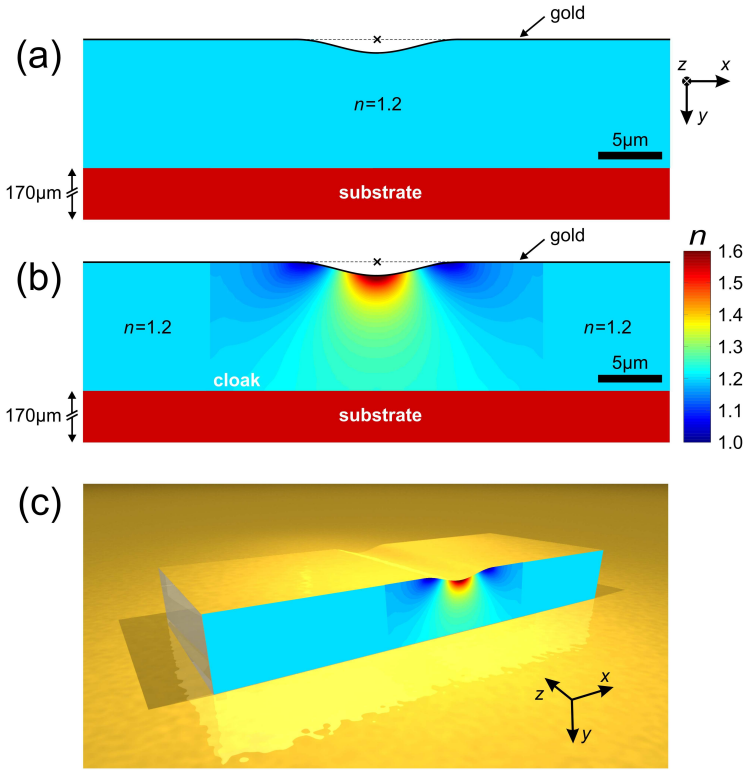

Fig. 1. (a) False-color representation of the refractive-index distribution of the reference structure within the *xy*-plane. Within the structure, the refractive index is constant along the *z*-direction. The structure is located on a thick glass substrate. The sample rotation axis is parallel to the *z*-direction and located at the depicted black cross. (b) Same as (a), but for the carpet cloak structure. On the left- and right-hand side, the cloaking structure is surrounded by regions of constant refractive index equal to the reference refractive index of n = 1.2. (c) Three-dimensional illustration of the overall structure in (b).

3. Ray tracing

We have previously published photorealistic images of sceneries including three-dimensional carpet cloaks using dedicated home-made ray-tracing software [12]. In the present contribution, aiming at a direct comparison with experiment [13], we rather want to model the bump in the metallic carpet, the cloaking structure, as well as the entire microscope and its illumination. The geometry is identical to that of the experiment shown in Fig. 2. Precisely, the illumination source emits isotropically distributed and randomly generated light rays or "photons" either from a point source or from a homogeneous disk with finite diameter d (composed of a homogeneous distribution of point sources). This light is collected via a first (condenser) lens and is sent onto the sample via an objective lens. Both lenses are taken as ideal (i.e., no chromatic and no spatial aberrations), are infinitely thin, and obey the usual lens equation. For the objective lens, the lens equation reads

$$\frac{1}{a}+\frac{1}{a'}=\frac{1}{f}. \qquad (1)$$

This lens with focal length f delivers a magnified image of the sample, which is held at distance a from the lens. a' is the distance of the image plane, in which all below images are computed. For ray tracing, we need an explicit expression for the angle α' of the ray emerging after the lens as a function of the incident angle α and the distance b between the ray and the

#133154 - $15.00 USD Received 10 Aug 2010; revised 1 Sep 2010; accepted 2 Sep 2010; published 10 Sep 2010

optical axis at the position of the lens with respect to the optical axis. From Eq. (1) and Fig. 2, it immediately follows that

$$\alpha' = \arctan\left(\frac{b}{f} \mp \tan(\alpha)\right). \tag{2}$$

The sign in Eq. (2) is dictated by the geometrical nature of the ray under consideration. As in the experiment, the magnification factor, m, is set to

$$m = 1 - \frac{a'}{f} = -80. \tag{3}$$

Hence, we have $a'/f = 81$ and $a/f = 81/80$. With the focal length of the objective lens $f = 5.41$ mm and its aperture radius of $r = 3.12$ mm, its numerical aperture NA follows as

$$NA = \sin(\varphi) = 0.5. \tag{4}$$

φ is half the opening angle of the lens, i.e., the maximum angle a ray may include with the optical axis (see Fig. 2). Rays outside of the lens' aperture are disregarded and, hence, do not contribute to the calculated images. The value of $NA = 0.5$ for the objective lens corresponds to a full opening angle of $2\varphi = 60$ degrees. The numerical aperture of the condenser lens is taken as 0.3.

We also explicitly account for the $t_s = 170$-µm thick glass substrate with refractive index $n_s = 1.545$ underneath the cloaking structure (see Section 2). The presence of the substrate defocuses the image if the objective lens is adjusted according to Eq. (1). To correct for this defocus, the sample has to be moved further away from the objective lens (i.e., $a \rightarrow a + a_s$) by a shift a_s along the optical axis. For rays including a small angle with the optical axis, a straightforward calculation yields the angle-independent result

$$a_s = t_s\left(1 - \frac{1}{n_s}\right), \tag{5}$$

leading to $a_s = 60$ µm. In contrast, for rays including larger angles with the optical axis, the defocus does depend on the angle. This aspect reflects the well known fact that a dielectric plate introduces spatial aberrations in an otherwise ideal optical microscope.

The distance from the illumination source that is centered on the optical axis to the condenser lens is 44 mm, the total distance from the condenser to the objective lens is 400 mm (compare Fig. 2).

Finally, the bump (with and without cloak) is centered with respect to the optical axis. We use the actual physical dimensions of the cloak as quoted above as well as the design refractive-index distribution of the cloak or the reference structure, respectively (see Fig. 1). Regarding ray tracing inside the cloak, we proceed as previously [12]: The continuously varying refractive-index distribution of the cloaking structure is discretized into $2000 \times 5200 \approx 10^7$ elements (elongated cuboids) with constant and wavelength-independent refractive index within each element. When passing an interface, the rays obey Snell's law. The

#133154 - $15.00 USD Received 10 Aug 2010; revised 1 Sep 2010; accepted 2 Sep 2010; published 10 Sep 2010

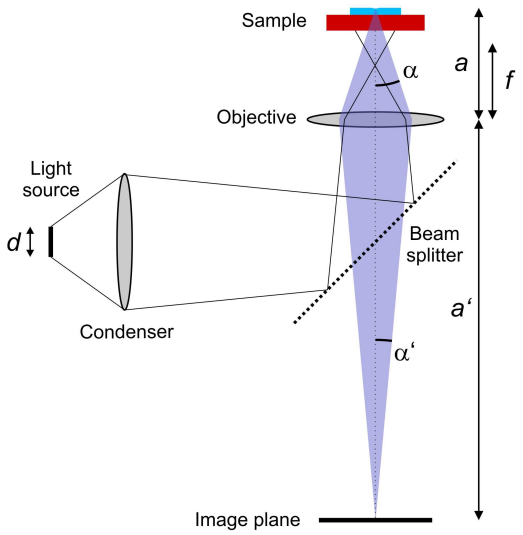

Fig. 2. Sketch of the microscope geometry (not to scale) used in our ray-tracing calculations of the 3D carpet cloak. The illumination light source is either a point source or a homogeneous disk with diameter *d*. For all images shown in this work, we focus the microscope onto the flat metal film on top of the polymer structure on the glass substrate. A magnified view of the sample is shown in Fig. 1.

reflections at the interfaces between discretization elements have to be treated with caution: partial Fresnel reflections should not occur in a continuously varying refractive-index profile. Hence, they are neglected.

In contrast, total internal reflections at the interfaces between discretization elements can occur. One illustrative example is a ray that enters from the left in the *xy*-plane shown in Fig. 1 propagating towards the right almost parallel to the metal film and that would hit the bump if there were no cloak. This ray bends downwards due to the refractive-index profile shown in Fig. 1(b). When this ray arrives in the middle of the bump, it bends upwards again due to the gradient of the refractive-index profile along the vertical direction (here the index decreases when going down). This behavior is very closely similar to that of rays in a mirage. The mentioned ray exits to the right nearly parallel to the metal film. If the discretization cuboids in this 2D problem are aligned along the *x*- and *y*-directions, the turning point of the ray corresponds to total internal reflection at the horizontal interface between two cuboids. (Confusingly, for differently oriented or differently shaped discretization elements, no total internal reflection may occur at this point, yet it may occur at others. The ray path eventually has to be independent of the discretization scheme.) Hence, total internal reflections at the discretization element interfaces have to be accounted for.

Partial Fresnel reflections at the physical interfaces (cloak/air, cloak/glass, and glass/air) are neglected. They have previously been shown to be of minor importance [12]. However, for angles beyond the critical angle, total internal reflections at these interfaces are again accounted for. In other words, no ray disappears or splits into two; any ray is either completely transmitted or completely reflected at any of the interfaces.

The presence of the cloaking structure or the reference structure (see Fig. 1), respectively, introduces an additional defocus similar to the defocus by the glass substrate according to Eq. (5). For a reference refractive index of $n_c = 1.20$ as in Fig. 1 and for a cloak thickness of $t_c = 10\ \mu\text{m}$ (see Section 2), we get in analogy to Eq. (5)

$$a_c = t_c\left(1-\frac{1}{n_c}\right), \tag{6}$$

#133154 - $15.00 USD Received 10 Aug 2010; revised 1 Sep 2010; accepted 2 Sep 2010; published 10 Sep 2010

leading to a_c = 1.7 µm. To correct for the overall defocus by substrate and structure, we have to replace the distance a obtained from Eq. (1) by $a \rightarrow a + a_s + a_c$ = 5.4776 mm + 60 µm + 1.7 µm = 5.5393 mm. The validity of this analytical focus condition has also been checked within our numerical ray-tracing calculations for both the uncloaked reference structure as well as for the cloaked structure.

4. Computational results without cloak

To get acquainted with the scenery and with the ray-optics images, Figs. 3 and 4 exhibit a variety of computational results for bumps without any cloaking structure. Results for a $\cos^2$-shaped bump like in Ref. 13 (also see Section 2) as well as for a triangular shaped bump as in Ref. 14 (width 13 µm and height 1.25 µm) are shown. Furthermore, we show illumination by a fictitious but conceptually simple point light source (Fig. 3) and by a more realistic disk-shaped light source with diameter d = 5 mm (Fig. 4). In all these cases, we depict the entire sample, the edges of which are visible by "scattering" of light off the sample edges. Precisely, these structures in the images originate from light rays impinging under nearly normal-incidence conditions that are totally internally reflected at the sample boundaries. These total internal reflections are the ray-optics counterparts of scattering of light off the sample edges in a wave-optics treatment.

For the point-source case, the images become completely dark for sample angles beyond a certain critical angle. This is obviously an artifact of the point-source approximation in Fig. 3. In sharp contrast, for the case of an extended light source in Fig. 4, scattering does occur in the dark-field mode for large angles – in agreement with our previous experiments [13]. Note that the bright-field images for point source and extended source are considerably different as well. The calculations for the disk-shaped source qualitatively agree with experiment [13]. These findings highlight the importance of using finite-size light sources in our calculations for obtaining results that can be compared with experiment in a meaningful manner. Hence, we restrict ourselves to finite-size illumination sources in the cases *with* cloaking in Section 5.

Nevertheless, the point-source case in Fig. 3 helps in understanding certain aspects: For example, a double-minimum structure is observed around the bright center for the $\cos^2$-shaped bump in bright-field mode. On the two sides, dark stripes occur. We have argued intuitively [13] that these dark stripes around the center maximum are due to light rays that are reflected off the two side slopes of the bump and not collected by the microscope objective lens. In contrast, light rays hitting the $\cos^2$-shaped bump's top with horizontal tangent are reflected just like from a flat mirror. Hence, they appear bright. It is interesting to check this interpretation on the triangular bump. Here, following this reasoning, one would obviously *not* expect a bright stripe in the middle because of the sharp triangle tip. Yet, one still gets a pronounced bright stripe – notably with a finite width. Indeed, a more complete interpretation also has to comprise the following aspects: Light rays reflected off the two side slopes of the triangular bump exit with a different angle compared to a flat mirror. For the present conditions, many of these rays are still collected by the objective lens. The fraction of the collected rays clearly depends on the numerical aperture (we will come back to this aspect in Section 5). Due to the different angle of the rays reflected off the bump (i.e., outside of the flat metal plane that is focused on), these rays appear laterally shifted in the image plane. The reflection off the left triangle side slope is shifted to the right, the reflection off the right triangle side slope to the left. In the middle, these shifted plates overlap, giving rise to the bright center stripe. The shifted plates leave behind darker areas. Only for much steeper bumps, most light rays get reflected such that they are no longer collected by the objective lens. We have also checked this interpretation by studying triangular bumps with fixed width but varying height (not depicted).

#133154 - $15.00 USD Received 10 Aug 2010; revised 1 Sep 2010; accepted 2 Sep 2010; published 10 Sep 2010

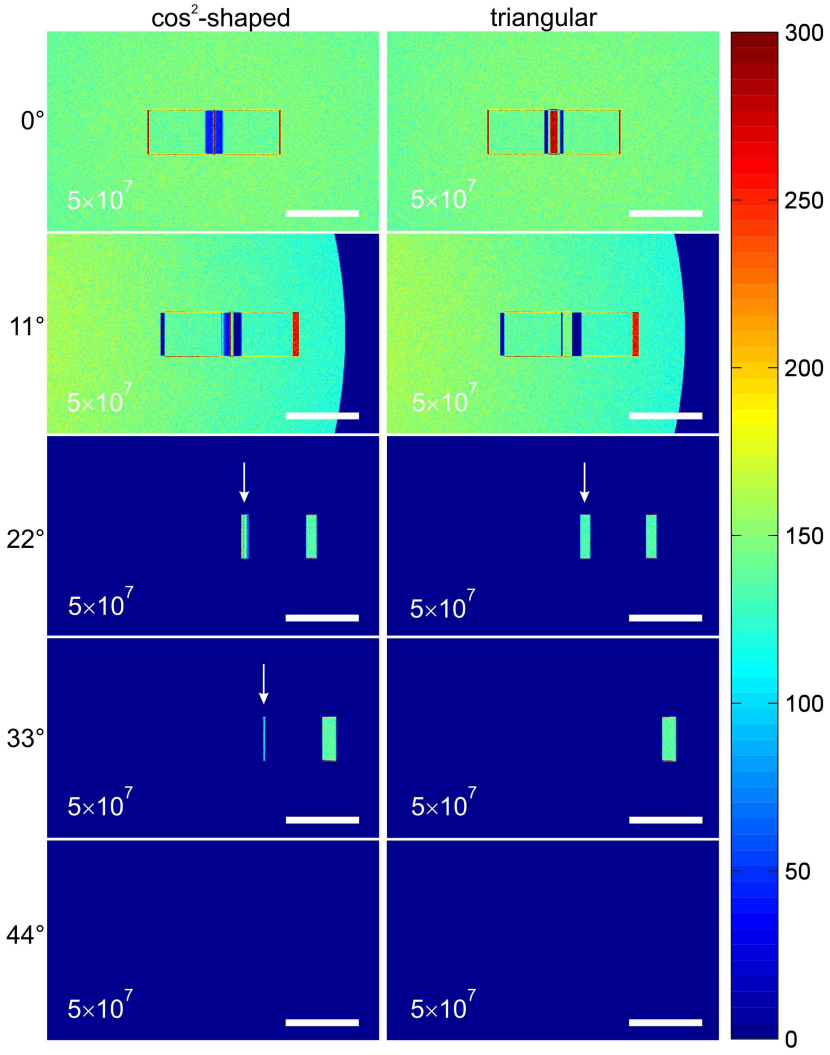

Fig. 3. Microscope images rendered by ray tracing for the geometry outlined in Fig. 2 and for the case of a bump *without* cloak (see Fig. 1(a)) and for point-source illumination. Images are shown for a $\cos^2$-shaped bump (left column) and for a triangular bump (right column). The five rows show different sample tilt angles increasing from top to bottom. Zero-degree tilt angle corresponds to the bright-field mode, large angles to the dark-field mode. The local image intensity is false-color coded. The values quoted on the right-hand side correspond to the total number of rays that have hit a square pixel element in the image plane, the area of which corresponds to 0.5 µm × 0.5 µm in the sample plane. The total number of rays that have illuminated the sample through the objective lens is given by the white number in the individual panels. The white scale bar shown in all panels corresponds to 50 µm length in the sample plane. The white arrows point to the scattering of light off the bump. Within the ray-optics approximation, the depicted images do not depend on wavelength at all.

#133154 - $15.00 USD Received 10 Aug 2010; revised 1 Sep 2010; accepted 2 Sep 2010; published 10 Sep 2010

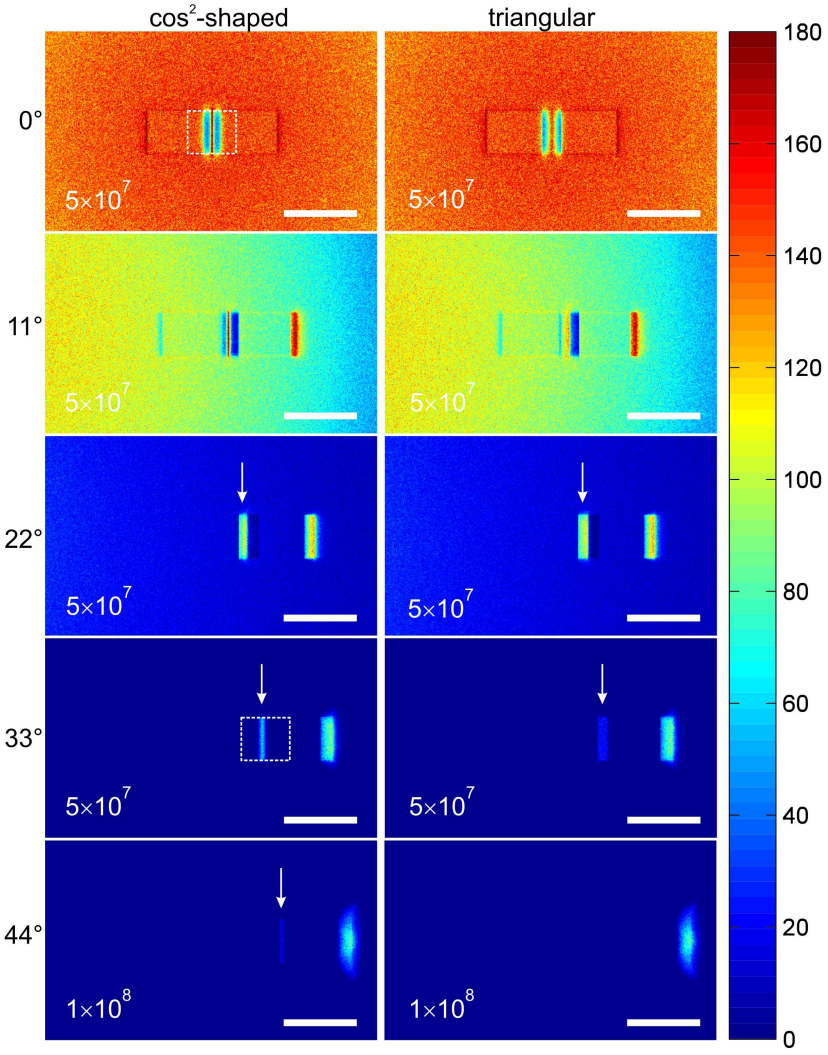

Fig. 4. Rendered microscope images as in Fig. 3, but for a finite disk-shaped light source with diameter d (see Fig. 2) rather than for point-source illumination. The dashed white rectangles outline the depicted areas in Figs. 5 and 6.

Along these lines, it also becomes clear why the bright center stripe for the $\cos^2$-shaped bump for the point-source case is much brighter than the reflection from the flat mirror regions on the sides: Due to the curvature (hence varying slope) of the side slopes, one no longer gets shifted plates as in the triangle case, but rather inhomogeneously compressed shifted plates that overlap in the middle, giving rise to the very bright center maximum. All of these features not only appear for the point-source case but also for the case of a finite illumination source (Fig. 4). There, however, they get smeared out considerably.

For the dark-field mode, no major qualitative differences occur between the images of the $\cos^2$-shaped bump and the triangular bump. The scattering off the bump (marked with white arrows in Figs. 3 and 4) merely disappears at smaller angles for the triangular shape than for the $\cos^2$ shape. This finding can be traced back to the fact that the maximum slope of the $\cos^2$ bump is $\pi/2$ times larger than the slope of the triangle.

#133154 - $15.00 USD Received 10 Aug 2010; revised 1 Sep 2010; accepted 2 Sep 2010; published 10 Sep 2010

5. Computational results with cloak

Let us now turn to the case with cloak. Following the above discussion for the case without cloak, we restrict ourselves to illumination with a disk-shaped light source and to $\cos^2$-shaped bumps with the dimensions given in Section 2. The refractive-index distributions used for the cloak and for the reference structure are shown in Fig. 1(a) and (b), respectively. Furthermore, to allow for a better comparison with our previous experimental results [13], we do not show images of the entire structure with all of its edges like in Figs. 3 and 4, but rather concentrate on the relevant central part with bump and cloak or the part that shows the bright scattering off the tilted bump, respectively. These depicted areas in Figs. 5 and 6 are outlined as dashed rectangles in Fig. 4. Figure 5 summarizes results for the bright-field mode (0-degree sample tilt) and for the dark-field mode (35-degree sample tilt as in Ref. 13). In each case, the uncloaked reference structure (also see Fig. 1) calculated under identical conditions shown right above the cloaked structure serves for direct comparison. In particular, as discussed in detail in Section 3, both the uncloaked and the cloaked structure are, of course, in focus.

For the bright-field mode in Fig. 5, excellent cloaking action is observed. With cloak, one nearly gets a homogeneous bright image as expected from a flat metal mirror. Cloaking has not been quite as perfect within the bright-field mode of our previous corresponding experiments [13], indicating that fabrication imperfections and/or using the inhomogeneous woodpile photonic crystal to mimic the refractive-index distribution may have played a certain role.

For the dark-field mode also depicted in Fig. 5, the cloaking performance is excellent as well. The bright scattering off the bump without cloak almost completely disappears with cloak. It is reduced by more than one order of magnitude and is therefore not visible on the depicted scale. The much dimmer bright stripe in the cloaked case has a different origin. As shown in Fig. 1, we have expanded the lateral extent of the structure by adding to the refractive-index profile derived from the quasi-conformal mapping a region of constant refractive index (equal to the reference refractive index of 1.2) to the left and to the right. The resulting index discontinuity at the interfaces is fairly small but still finite. In close analogy to the "scattering" from the structure side walls already described in Section 4, we again get total internal reflection of certain light rays due to this discontinuity. These discontinuities are also visible as small intensity variations on the left and right edges in bright-field mode. In the corresponding experiments [13], these fine details have not been visible as they have very likely been smeared out by the photonic-crystal nanostructure that mimics the refractive-index profile. We conclude that cloaking of the carpet cloak is close to perfect in the dark-field mode within our ray-optics treatment – in good agreement with our corresponding experiments [13].

The bright-field mode calculations shown in Fig. 5 have been for an objective lens numerical aperture of $NA = 0.5$ ($2\varphi = 60$ degrees). It is interesting to ask whether the results are modified for a yet larger NA. A larger numerical aperture means that the structure is probed by rays from even more directions in three-dimensional space. Unity NA would correspond to a full opening angle of the cone of light of $2\varphi = 180$ degrees. Results for $NA = 0.7$ ($2\varphi = 89$ degrees) and $NA = 0.9$ ($2\varphi = 128$ degrees) are shown in Fig. 6. All other parameters are identical to those in Fig. 5. We only show the bright-field mode in Fig. 6 because a flat mirror no longer appears completely dark for sample angles of 35 degrees (Fig. 5) at such large numerical apertures (also compare Figs. 3 and 4 for smaller angles). The contrast in the bright-field images for the uncloaked case decreases with increasing numerical aperture from $NA = 0.5$ in Fig. 5 to $NA = 0.7$ and $NA = 0.9$ in Fig. 6. As discussed in Section 4, the two dark stripes at the side walls of the bump are partly due to rays that are not collected by the microscope objective lens. Clearly, more rays are collected for higher numerical aperture, leading to filling up of the two minima. Hence, the contrast in the images is reduced.

#133154 - $15.00 USD Received 10 Aug 2010; revised 1 Sep 2010; accepted 2 Sep 2010; published 10 Sep 2010

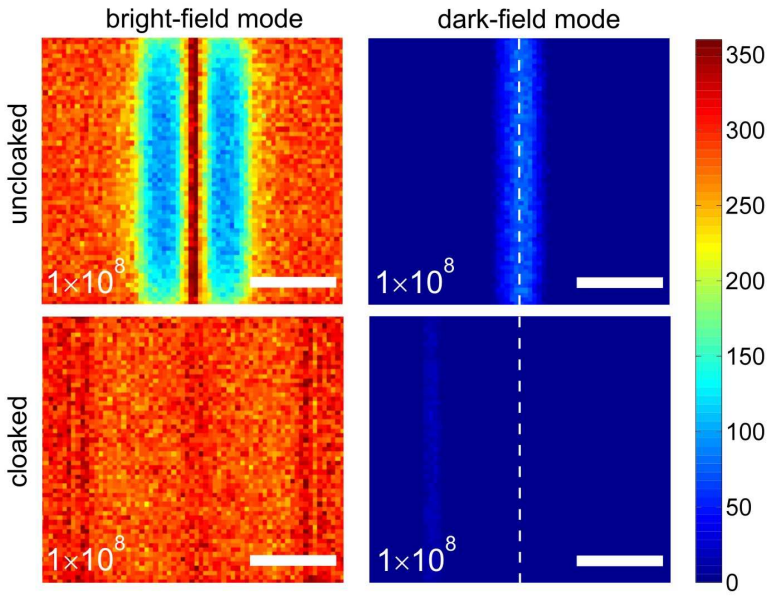

Fig. 5. Microscope images for the bright-field mode (left column) and the dark-field mode with 35-degree sample tilt (right column) without (first row) and with carpet cloak (second row), all rendered by ray tracing. The structure dimensions are given in Sections 2 and 3, the objective lens numerical aperture is *NA* = 0.5 (see Fig. 2). The refractive-index distribution underlying the carpet cloak is shown in Fig. 1. A total number of 10^8 rays have illuminated each sample. The scale bar corresponds to a length of 10 μm in the sample plane. The area of the image shown here is outlined in Fig. 4. The dashed white line marks the position of the bump reflection in both dark-field images.

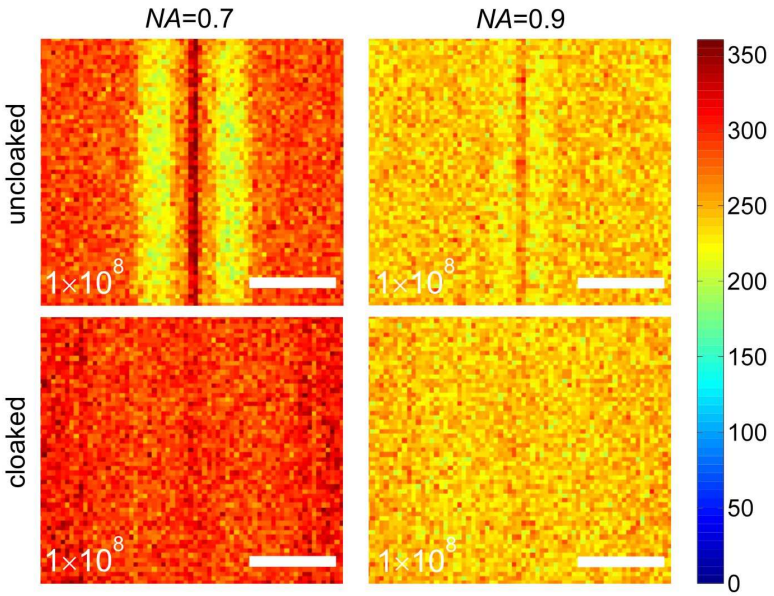

Fig. 6. Microscope bright-field images as in the left column of Fig. 5 (with *NA* = 0.5), but for a numerical aperture of the objective lens of *NA* = 0.7 and *NA* = 0.9 as indicated (see Fig. 2). For these cases, the light samples a much larger fraction of all possible directions in three-dimensional space.

#133154 - $15.00 USD Received 10 Aug 2010; revised 1 Sep 2010; accepted 2 Sep 2010; published 10 Sep 2010

Obviously, the cloaking performance in Fig. 6 remains excellent. One should, however, also bear in mind that the spatial imaging aberrations introduced by the dielectric glass substrate in the optical path of the microscope (as discussed in Section 3) are expected to play a certain role at such large numerical apertures. These aberrations may obscure the images to some extent.

6. Conclusions

We have presented ray-tracing calculations on three-dimensional carpet cloaks imaged by unpolarized light using an optical microscope with large numerical aperture in bright- and in dark-field optical modes. The calculated images can be directly compared with our recently published experimental results [13], leading to good overall qualitative agreement. This finding indicates that the experiments are on the right track towards macroscopic invisibility cloaks, for which the rules of geometrical optics and effective media should apply. The recently emphasized intrinsic limitations of the carpet (or ground-plane) cloak without anisotropy seen in 2D ray-tracing calculations [15] do not appear to play a major role in our 3D ray-tracing calculations of the microscope images.

Analogous 3D ray-tracing calculations might help us in designing future experiments on three-dimensional transformation-optics structures operating at optical frequencies.

Acknowledgements

We thank Joachim Fischer for valuable discussions. We acknowledge support by the Deutsche Forschungsgemeinschaft (DFG) and the State of Baden-Württemberg through the DFG-Center for Functional Nanostructures (CFN) within subprojects A1.4 and A1.5. The project PHOME acknowledges the financial support of the Future and Emerging Technologies (FET) programme within the Seventh Framework Programme for Research of the European Commission, under FET-Open grant number 213390. The project METAMAT is supported by the Bundesministerium für Bildung und Forschung (BMBF). The Ph.D. education of T. Ergin is embedded in the Karlsruhe School of Optics & Photonics (KSOP), and N. Stenger is supported as a Mentor in KSOP. T. Ergin and J. C. Halimeh contributed equally to this work.

#133154 - $15.00 USD Received 10 Aug 2010; revised 1 Sep 2010; accepted 2 Sep 2010; published 10 Sep 2010